ELSEVIER

Journal of Chromatography A, 733 (1996) 105–117

JOURNAL OF CHROMATOGRAPHY A

Determination of adsorption characteristics of the nutrient orthophosphate to natural colloids by sedimentation field-flow fractionation

Jason van Berkel, Ronald Beckett*

CRC for Freshwater Ecology and Water Studies Centre, Department of Chemistry, Monash University, P.O. Box 197, Caulfield East, Vic. 3145, Australia

Abstract

The surface adsorption density distributions (SADD) for ^{32}P-labelled orthophosphate onto a suspended river colloid and a soil colloid were determined by the sedimentation field-flow fractionation (SdFFF) method. The surface adsorption density (SAD) was not constant with particle diameter as expected for homogeneous solids and were quite different for the two samples.

The shape of particles was determined by examining separated fractions using scanning electron microscopy (SEM). A procedure was developed for correcting the SAD, which is normally calculated assuming constant spherical shape, for changes in morphology from spheres to plates or rods having different aspect ratios. It was shown that shape can have a large effect on the SADD plot.

Changes in chemical composition across the size distribution were measured using on-line SdFFF–inductively coupled plasma-mass spectrometry. Significant trends in the Fe/Al and Mg/Al atomic ratios as a function of size were observed. These element distributions can help explain the trends in the SADD plots which could occur due to a variation in the hydrous iron oxide surface coating thickness or by changes in the mineralogy of the sample. The methodology gives very detailed adsorption data which yields insights into the nature of the pollutant–colloid binding in waters and soils.

Keywords: Environmental analysis; Adsorption density distribution; Surface adsorption density distribution; Pollutant–colloid binding; Colloids, natural; Field-flow fractionation; Soil; Water analysis

1. Introduction

There is increasing environmental concern about the occurrence of algal blooms in aquatic systems. The deleterious effects of such outbreaks of cyanobacteria include oxygen depletion in the water column, reductive release of contaminants from anoxic sediments and the production of toxins that can cause stock and wildlife losses as well as human health problems. One of the factors thought to be responsible for algal blooms is the excessive release of the plant nutrient phosphorus into waterways from sources such as sewage, industrial and domestic wastewaters and agricultural run-off due to fertiliser use and intensive animal farming.

In aquatic systems phosphorus can exist in many forms including orthophosphate, condensed inorganic phosphates, organophosphorus esters and associated with both inorganic particles and biota. The most readily available form of phosphorus is the simple orthophosphate ion; however, in many systems the largest pool of phosphorus is found associ-

*Corresponding author.

0021-9673/96/$15.00
SSDI 0021-9673(95)01076-9

ated with colloidal particles. It is not certain whether cyanobacteria can readily utilize much of the orthophosphate bound to suspended particles. The work reported in this paper is part of an ongoing program to develop methods that will help elucidate the factors responsible for causing strong adsorption of orthophosphate to natural particles in waters, sediments and soils. In addition, the distribution of strongly bound orthophosphate across the size spectrum of a colloidal sample will affect the transport and fate in both aquatic environments and through soils and ground water.

In previous publications Beckett and coworkers have developed methods based on sedimentation field-flow fractionation (SdFFF) for studying pollutant–colloid interactions [1] and for performing detailed physical and chemical characterization on soil and water-borne particles [2–4].

SdFFF is an elution based separation and sizing method founded on well understood physical principles [5]. The sample is injected into a thin unpacked channel and subjected to the combined influence of a centrifugal field force and the laminar parabolic fluid flow profile directed along the channel and at right angles to the field (Fig. 1). In the normal mode of operation the result is that particles are separated and eluted from the channel in the order of increasing effective mass. The mass concentration of sample in the effluent is monitored using a UV detector and fractions can be collected for analysis. Using well established equations the time for particles to migrate through the channel can be converted to a corresponding equivalent spherical diameter [1,6]. Thus the particle size distribution can be computed from the experimental fractogram [4].

If the eluent stream can undergo continuous elemental analysis then element based size distributions can be also computed. This is feasible using

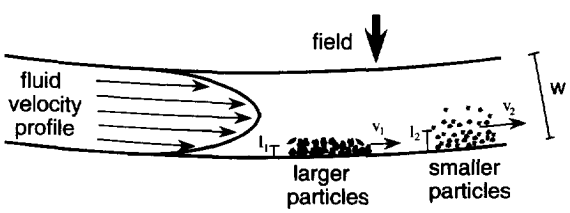

Fig. 1. A schematic diagram of a sedimentation FFF channel.

inductively coupled plasma-mass spectrometry (ICP-MS) and the elemental size distributions and element molar ratio distribution are valuable in monitoring changes in mineralogy across the size distribution [7]. Further information on the chemical trends within the particles can be obtained from electron photomicrographs of fractions collected across the fractogram [3]. This yields morphological data such as the equivalent circular cross-sectional diameter: particle thickness ratio (plate aspect ratio) or the equivalent circular cross-sectional diameter (d_d): equivalent spherical diameter (d_s) ratio (geometric diameter ratio). This data can help identify particles on the basis of the characteristic shape of certain minerals [8].

A powerful methodology using SdFFF has been developed recently for studying pollutant–colloid binding [1]. In this work it involved adsorbing radiolabelled orthophosphate onto colloidal particles and then sizing and separating them by means of SdFFF. A series of fractions are collected as a function of elution time and their radioactivity measured. From these measurements the distribution of the adsorbed orthophosphate can be calculated as a function of particle size. Such plots are significant in determining the mode of transport and fate of pollutants in natural aquatic and soil systems.

This approach also enables the surface adsorption density distribution (SADD) of the pollutant (orthophosphate in this work) to be determined for a given particulate sample. A SADD is a plot of the amount of adsorbate per unit area of particle surface as a function of particle size. Thus for a chemically homogeneous sample the SADD should be constant across the entire size range. A nonconstant SADD may occur if there is a change in mineralogy or surface coating density across the distribution. In addition since the calculations utilized to date involve assuming a constant particle shape (usually spherical), texture, porosity and density, these properties can also influence the observed trends in the SADD plots.

This paper reports on an initial study in which SdFFF–ICP-MS element composition and element molar ratio distributions and SdFFF–SEM particle shape data are combined to help interpret the origin of nonconstant orthophosphate–natural colloid SADD curves. The longer-term aim is to develop the

SdFFF–SADD methodology into a useful tool for determining the nature of pollutant–particle association in waters and wastewaters.

2. Theory

2.1. Sedimentation field-flow fractionation

SdFFF is a set of high-resolution liquid chromatography-like elution methods used for sizing and separating colloidal matter into size fractions. SdFFF separations are performed within a flat open channel, usually having a rectangular cross-section and triangular end pieces where the sample and carrier fluid enters and leaves (see Fig. 1). SdFFF has excellent resolution but can only process small quantities (<1 mg) of sample in a single run [1,3,4,7,9].

The mechanism for particle separation involves only physical interactions [4]. The sample is introduced into the channel through a septum or injection valve, and then the flow is turned off. A centrifugal field is then applied at right angles to the flat face of the ribbon-like channel. This flat channel sits within a centrifuge basket and the centrifugal field drives the particles towards the accumulation wall. There they form equilibrium clouds whose average thickness or elevation above the accumulation wall (l) depends on how strongly the particles interact with the field and also their diffusivity [1,3,4,9].

When the carrier liquid flow is turned on at the end of the stop-flow (relaxation) period, the run begins. The carrier flow in the thin flat channel is laminar with the linear fluid velocity being zero at the channel walls and increasing with distance away from each wall, thus approaching a maximum at the centre of the channel. The particles with a larger effective mass will have more compressed sample clouds (i.e. a smaller l) and will consequently be swept down the channel by the flow at a lower average velocity than the smaller particles. In this normal mode of SdFFF the smallest particles will elute first [7].

The retention ratio R, for a constant field normal mode FFF run is obtained from the measured elution volume V_r and channel void volume V^0 according to the expression:

$$R = \frac{V^0}{V_r} = 6\lambda\left(\coth\frac{1}{2\lambda} - 2\lambda\right) \quad (1)$$

where $\lambda = l / w$, with l being the cloud thickness and w being the channel thickness. The equivalent spherical particle diameter, d, can be calculated from λ provided the density difference between the particle and the carrier liquid $\Delta\rho$ is known [7]. The expression used is:

$$d = \sqrt[3]{\frac{6\,kT}{\pi\omega^2 rw\Delta\rho\lambda}} \quad (2)$$

where k is the Boltzmann constant, T the absolute temperature, w the centrifuge speed (radians s^{-1}) and r the centrifuge radius.

For samples which contain a broad size distribution the field decay program strategy of Williams and Giddings can be used [5,6]. This program uses an initial constant speed ω_0 for a period t_1, after which the centrifuge speed decays according to the power equation:

$$\omega = \omega_0\left(\frac{t_1 - t_a}{t - t_a}\right)^4 \quad (3)$$

where t_a is a constant that controls the rate of decay and t is the run time. This enables the smaller particles to be adequately resolved from the void peak utilizing the higher field strength period while avoiding excessively long retention times for the larger particles. The run can be optimised to achieve a desired level of resolving power across the size range if suitable values of ω_0, t_1, t_a and flow-rate are used [7].

2.2. Fractograms

SdFFF usually utilizes an ultraviolet (UV) detector operating at a wavelength of 254 nm to monitor the sample concentration. The UV detector generates a particle mass based fractogram which is a plot of the mass concentration of particles (dm' / dV_r), as monitored by the UV absorbance signal (UV) eluting as a function of elution time (t_r) or volume (V_r) [1]. Where m' is the correlative mass of particles eluted up to a given elution volume. It is recognised that there will be some uncertainties in the measured eluent concentration due to the dependence of the

detector signal on the particle size, as the light attenuation in this situation is mostly due to scattering rather than absorption [1].

The mass concentration of selected elements (E) can be determined experimentally by using an inductively coupled plasma-mass spectrometer (ICP-MS). The SdFFF eluent is fed into the ICP-MS instrument and an ion current I_E is generated, which is proportional to the mass concentration of the elements present in the sample (i.e. dm'_E / dV_r). Again m'_E denotes the cumulative mass of element E eluted up to volume V_r. Therefore element mass based fractograms can be obtained by plotting the element concentration ($d'm_E / dV_r$) versus t_r or V_r.

2.3. Mass based size distributions

By using Eqs. 2 and 3 the equivalent spherical particle diameter corresponding to a given elution volume can be calculated if the run is assumed to be made up of a large number of constant field increments stepping down from ω_0 as the field decays. The fractogram obtained above can then be manipulated to produce a particle mass based size distribution which is a plot of (dm' / dd) versus diameter (d).

In order to obtain the correct ordinate for the mass based size distribution ($dm'_{(i)} / dd_{(i)}$), the volume-axis of the fractogram is divided into a large number of increments of width $\delta V_{(i)}$, and the following equation is used:

$$\frac{dm'_{(i)}}{dd_{(i)}} = \left(\frac{dm'_{(i)}}{dV_{(i)}}\right) \times \left(\frac{\delta V_{(i)}}{\delta d_{(i)}}\right) \propto UV_{(i)} \times \frac{\delta d_{(i)}}{\delta V_{(i)}} \qquad (4)$$

where $dm'_{(i)} / dV_{(i)}$ is the value of the fractogram ordinate at the midpoint of a given volume increment $\delta V_{(i)}$, and $\delta d_{(i)}$ is the diameter increment corresponding to the same increment in V. The UV detector signal at point i ($UV_{(i)}$) is substituted for $dm'_{(i)} / dV_{(i)}$ to plot the particle size distribution [1,3]. The area under the particle size distribution between any two values of d represents the mass of particles in that particular size range.

The element based fractograms can similarly be converted into element mass based size distributions i.e. $dm'_{E(i)} / dV_{(i)}$ versus $d_{(i)}$. The different elemental data can be combined to give atom (or molar) ratio plots versus particle diameter, which are a good indication of any change in mineralogy across the size range [7].

2.4. Surface adsorption density distribution

A scintillation counter was used to monitor concentration of adsorbed orthophosphate in the SdFFF eluent ($dP_{(i)} / dV_{(i)}$). The amount of pollutant P (i.e. radiolabelled orthophosphate) adsorbed per unit mass of adsorbent at any point (i) along the elution time or elution volume axis is given by:

$$\frac{dP_{(i)}}{dm'_{(i)}} = \left\{ \left(\frac{dP_{(i)}}{dV_{(i)}}\right) \Big/ \left(\frac{dm'_{(i)}}{dV_{(i)}}\right) \right\} \propto \frac{DPM_{(i)}}{UV_{(i)}} \qquad (5)$$

where $DPM_{(i)}$ is the β activity in disintegrations per minute measured per ml of eluent.

As defined above a SADD plot is the amount of pollutant (P) adsorbed per unit area of particle surface ($dP_{(i)} / dA_{(i)}$), usually expressed in arbitrary units, as a function of particle diameter (d_i) [1,3]. If spherical particles are assumed the particle area ($dA'_{(i)}$) in an increment of elution volume ($dV_{(i)}$) is given by $6\delta m'_{(i)} / d_{(i)}\rho$. Therefore, assuming a sample of constant shape and density, a surface adsorption density at any diameter $d_{(i)}$ can be calculated using Eq. 6 which is derived using Eq. 5 and the sample geometric fact that $\delta m' / \delta A' = \rho d/6$. The expression for the SADD ordinate is:

$$\frac{dP_{(i)}}{dA'_{(i)}} = \left\{ \left(\frac{dP_{(i)}}{dm'_{(i)}}\right) \times \left(\frac{\delta m'_{(i)}}{\delta A'_{(i)}}\right) \right\} \propto \frac{DPM_{(i)}}{UV_{(i)}} \times d_{(i)} \qquad (6)$$

2.5. Influence of shape on the SADD

Since the calculations used to calculate the SAD have assumed a constant spherical shape, any change in shape would introduce discrepancies into the resultant SADD plot [1,3]. Consider a disc-shaped or platelet-shaped particle which elutes at the same time as a spherical particle. Both must have the same buoyant mass and if the density is the same, the volume must also be the same. Simple geometry can be used to derive an expression for the ratio of the

surface areas of the coeluting disc (A_d) and sphere (A_s) in terms of the geometric diameter ratio d_d / d_s. Thus:

$$\frac{A_d}{A_s} = \frac{1}{2}\left(\frac{d_d}{d_s}\right)^2 + \frac{2}{3}\left(\frac{d_s}{d_d}\right) \quad (7)$$

where d_d is equivalent circular cross-sectional diameter of the disc or rod and d_s is the diameter of a sphere with the same volume. Note that this expression is equally applicable for rod-like particles if we consider a rod as being a disc with d_d / $d_s < 1$.

In these cases the specific surface area of the plate and rod-like shapes is underestimated more and more as the shape deviates from the ideal spherical particle. This is clearly shown by the plot of Eq. 7 given in Fig. 2. The SAD is the amount of pollutant adsorbed per unit surface area and in these calculations spherical shape is assumed. If non-spherical particles are present a correction must be made to the ideal spherical particle SAD ($(dP_{(i)} / dA_{(i)})_{sphere}$).

For example, a change in shape from spherical particles to plate-like particles would give rise to an increase in the apparent SAD as the aspect ratio increases. Similarly, for cylindrical rods the calculated SAD would increase as the rod length/diameter ratio increases.

At each point i along the distribution the true SAD for the sample $(dP_{(i)} / dA_{(i)})_{sample}$ will be given by:

$$\left(\frac{dP_{(i)}}{dA_{(i)}}\right)_{sample} = \left(\frac{dP_{(i)}}{dA_{(i)}}\right)_{sphere} \Big/ \frac{1}{m}\sum_{j=1}^{m}\left(\frac{A_d}{A_s}\right) \quad (8)$$

where the denominator is the average A_d / A_s ratio of the m particles examined by SEM in the sample collected at point i along the fractogram. Since d_d can be obtained from SEM (although this will be somewhat tedious) and d_s so calculated from the SdFFF equations at the mid point of fraction i, A_d / A_s is given by Eq. 7, thus it should be possible to make appropriate corrections and obtain more exact SADD plots.

3. Experimental

3.1. Sample collection

Suspended particulate matter from the Darling River (New South Wales) and a soil sample from the Mount Lofty Ranges (South Australia) was studied. The A1 horizon soil sample was obtained from the Mount Lofty Ranges at a site located in the Onkaparinga catchment several kilometres northwest of the Mount Bold Reservoir. The soil suspension was then separated by centrifugation procedures to yield a fraction approximately 0.08–1 μm in diameter [2,10].

The Darling River water was sampled at Bourke. The sample was first passed through a continuous flow centrifuge to remove particles greater than about 1 μm. The supernatant was then concentrated about 100-fold using tangential flow filtration with Millipore polysulphone membrane filters of nominal cutoff, 0.2 μm. The concentrates were stored at 4°C

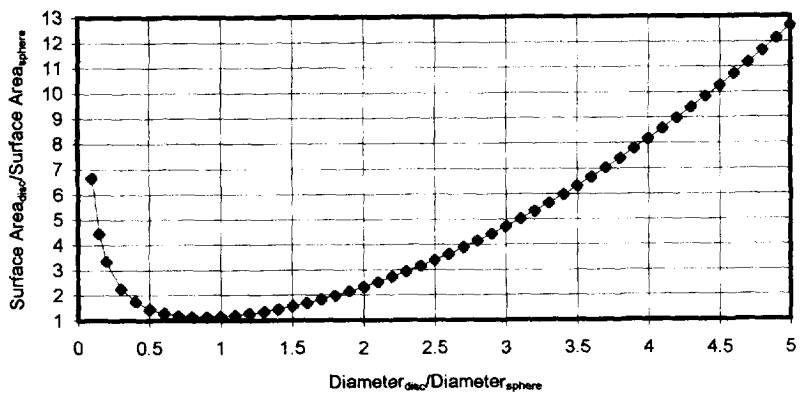

Fig. 2. A plot of ratio of area of a plate to the area of a coeluting sphere versus the ratio of the equivalent circular plate diameter to the diameter of a sphere.

and prior to use were subject to ultrasound to break up any aggregates present.

3.2. Adsorption experiments

3.2.1. Adsorption procedure

^{32}P-labelled orthophosphate in dilute hydrochloric acid (40 MBq) was obtained from The Australian Nuclear Science and Technology Organisation (ANSTO). An amount of 20 μl of $^{32}PO_4^{3-}$ was added to 1 ml of colloid concentrate and allowed to stand for 24 h before separation by SdFFF was commenced.

3.2.2. Analysis of activity

Fractions were collected over 5 min intervals. An amount of 1 ml of each fraction was added to 4 ml of scintillant (Ultima Gold) in a scintillation vial. After agitation in a vortex mixer, the raw data were measured for 10 min in a Beckmann LS6000TA scintillation counter (DPM). The raw data is converted into auto DPM values. Auto DPM allows dpm values for a single-labelled sample with a pure beta-emitting isotope (^{32}P) without running quench curves. The program uses default parameters set by the instrument. An auto DPM calibration is performed at the factory and the calibration stored.

3.3. Sedimentation field-flow fractionation

3.3.1. Apparatus

The SdFFF apparatus was similar to a Model S100 available from FFFractionation (Utah, USA). The SdFFF channel was made by clamping two concentric nickel–chromium-rich alloy (Hastalloy C) rings with a 0.0282-cm-thick mylar spacer (which had the channel shape cut out) sandwiched between them. The system 1 channel was 89.1 cm long (inlet to outlet) and 2.15 cm in breadth. The channel void volume was 4.91 ml. The channel was fitted inside a centrifuge basket so that its radius was 15.1 cm. The system 2 channel was 89.1 long (inlet to outlet) and 2.15 cm in breath. The channel void volume was 2.5 ml and the channel radius 15.5 μm. The channel width was 0.015 cm. O-ring seals at the ends of the axle allowed liquid to flow through the channel while the centrifuge rotated. The rotor was powered by a DC motor (Baldor permanent magnet servomotor) and speed controller. The rotation speed was controlled by in-house field-decay software.

The carrier solution was pumped by a MiltonRoy ConstaMetric III metering pump and the outlet stream was passed through a LDC Milton Roy SpectroMonitor variable wavelength detector operating at 254 nm. A Retriever 500 fraction collector was used to collect the samples at various elution times.

3.3.2. FFF run parameters

The required injection volume (Darling River 20 μl, Mt Bold A1 Soil 10 μl) was introduced onto the channel through a rubber septum with a syringe. The river colloid concentrates were relaxed at 1000 revolutions per minute (rpm) for 20 min under stop-flow conditions. The Mt Bold soil colloid concentrates were relaxed at 800 rpm for 20 min under stop-flow conditions. For system 1 this initial field strength was held for a lag time t_l of 10 min once the run started. A decay parameter t_a of -80 min reduced the field to a hold value of 20 rpm after approximately 100 min. For system 2, t_l was 4 min and t_a was -32 min.

For system 1 an aqueous solution of 0.1% (w/v) sodium dodecylsulphate and 0.02% (w/v) sodium azide at a flow-rate of 2 ml/min was used as the carrier. For system 2, an aqueous solution (w/v) $5 \cdot 10^{-4}$ M of tetrasodium pyrophosphate (SPP) and 0.02% (w/v) sodium azide at a flow-rate of 1 ml/min was used as the carrier. Detector sensitivity was held at 0.02 a.u.f.s. The chart recorder was held at 10 cm/h. Fractions were collected over 5 min intervals for the radioactivity and SEM/EDX measurements.

3.4. Scanning electron microscopy (SEM) and energy dispersive X-ray analysis (EDX)

A Hitachi S-2300 Model SEM was used to determine the shapes of the colloidal particles and to verify the accuracy of the SdFFF separations. EDX was used to determine the mineral composition of

the particles. The fractions collected every 5 min were filtered. Fractions less than 0.1 μm were filtered through a 0.05 μm Nucleopore filter and those fractions larger than 0.1 μm were filtered through a 0.1 μm Nucleopore filter. The filters were cut (approximately 0.5 cm×1cm) and attached to an aluminium stub. For SEM analysis the filters were coated with platinum. For the EDX analysis the filters were coated with carbon because platinum peaks appear in the same region as aluminium and silicon, the main elements expected in the particles. The SEM instrument was operated at 25 kV and at a magnification of ×20 000. The EDX instrument was operated at 20 kV and at a magnification of ×5000.

3.5. Inductively coupled plasma-mass spectroscopy apparatus (ICP-MS)

The SdFFF was directly coupled to a VG Plasmaquad ICP-MS in order to obtain high-resolution element distributions as a function of particle size. By using a t-piece after the UV detector and a peristaltic pump attached to the v-groove nebulizer of the ICP-MS, about half of the eluent from the SdFFF could flow into the ICP-MS and the remaining 50% could be collected with a fraction collector or go directly to waste. The internal standards present in the tetrasodium pyrophosphate (SPP) carrier were indium and/or cobalt to allow for noise and drift corrections. The standard stock mixture contained the following concentration of elements: 400 ppb Al, 200 ppb Fe, 50 ppb Mg, 10 ppb Mn, Ba, Sr and Pb, 5 ppb Cu, Cd, Zn and rare earths and 1 ppb Rb.

These standards were diluted two-fold (200 ppb Al), four-fold (100 ppb Al) and twenty-fold (20 ppb Al) with SPP carrier. An Excel macros program was used to perform element-by-element drift corrections and compute the element concentrations based on the above solution standards.

The ICP-MS run conditions were as follows: mass range 23.5 to 210.41 a.m.u.; number of scan sweeps 100 and the instrument operated in pulse-counting mode. The sample concentrates were diluted by a factor ×1000 before injection into the SdFFF–ICP-MS.

4. Results and discussion

4.1. Size distributions and surface adsorption density distributions

The particle size distributions show a broad peak from about 0.1 to 0.6 μm for both samples (Fig. 3b, c). The fact that particles less than the 0.2-μm cutoff for the Darling River sample are present is most likely due to partial pore blockage or aggregation occurring during filtration (see Fig. 3b).

The $^{32}PO_4^{3-}$ adsorption distributions given in Fig. 3b, c show that a significant amount of radioactive material is adsorbed to the particles. The smallest particles contained the highest adsorbate content which can be explained by the expected increase in specific surface area as particle size decreases and the fact that the size distributions have maxima at a quite small particle diameter (0.1–0.2 μm).

Fig. 3c, f show the surface adsorption density distributions (SADD) calculated from the respective UV and DPM fractograms given in Fig. 3a, d. The plots are a measure of the amount of adsorbate per unit area of particle surface as a function of particle size and are calculated assuming spherical geometry. The open circles on the SADD plots are computed using a shape correction factor (see Eq. 8) as discussed in the next section.

An ideal model for homogeneous colloidal samples would predict that the surface adsorption density distribution for a given pollutant–colloid system would be constant across the size range investigated. The SADD curves from the Darling River (Fig. 3c) and A1 Soil (Fig. 3f) display distinct differences. Both curves show an initial decrease in dP / dA as particle size d increased from 0.05 to 0.15 μm, after which the slopes for each sample deviate from each other. The Darling River SADD (Fig. 3c) showed an increase in dP / dA as particle size increased from 0.2 to 0.5 μm. This trend is particularly pronounced above 0.4 μm. In contrast the dP / dA values for the A1 Soil continued to decrease from 0.15 to 0.4 μm suggesting that the larger particles were adsorbing less orthophosphate per unit area than the smaller particles. However, these apparent trends in the SADD plots may be influenced by a change in the particle shape across the distribution as discussed below.

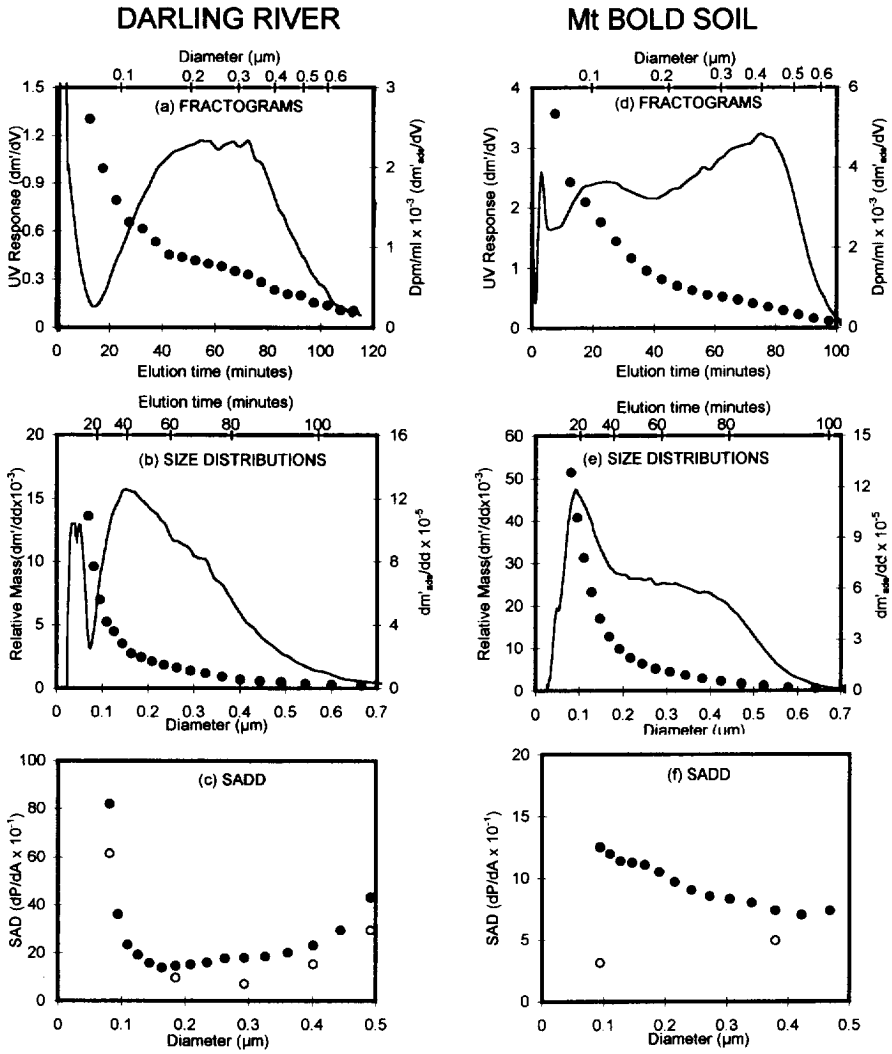

Fig. 3. (a) and (d) SdFFF fractograms (system 1) of natural colloid samples with adsorbed radiolabelled orthophosphate. The solid lines give the UV detector response and the points give the radioactivity (dpm/ml) in the effluent. (b) and (e) Particle mass based and adsorbate based size distributions. The solid lines give the Relative Mass of particles and the points give the amount of orthophosphate adsorbed (arbitrary units). (c) and (f) Surface adsorption density distributions. The closed circles give the amount of orthophosphate adsorbed per unit area of particle surface based on the assumption that all the particles are spherical in shape. The open circles are corrected for changes in shape as explained in text.

The phosphate adsorption data was only used for data points corresponding to a particle diameter greater than about 0.08 μm. This is well beyond the void peak which probably contains unabsorbed phosphate. Thus the SADD data in Fig. 3c, f reflects the amount of phosphate adsorbed to particles and there should not be any interference from material eluting in the void peak.

4.2. Analysis of shape with SEM

Inspection of the SEM photomicrographs showed that the Darling River sample contained some platelet-shaped particles, although they did not dominate the sample. By measuring the cross-sectional area of these platelets it is possible to use the SdFFF elution volume to estimate the particle thickness. For

example a particle collected at an elution time of 80–85 min had a cross-sectional area of 0.81 μm^2 with a SdFFF-predicted equivalent spherical diameter of 0.47 μm. The observed equivalent circular diameter is approximately 1.0 μm which gave a particle thickness of 0.067 μm. The aspect ratio (particle diameter/particle thickness) is 15 which indicates that the particle is a plate. From Eq. 7 the A_d / A_s ratio (surface area of a disc or a plate/ surface area of a coeluting sphere) for this particle with a d_d / d_s ratio of 2.1 (diameter of a disc/ diameter of a coeluting sphere) is 2.6. Therefore, due to the presence of platelet-shaped particles which appear to have a surface area 2.6 larger than a spherical particle of the same mass (see Eq. 7), the SADD plot in this size range could have a considerable error.

To access the influence of shape on the SADD plot a total of 55 particles in five fractions collected across the fractogram were analysed in this way. The results are summarised in Table 1. The shape of the particles, as indicated by the aspect ratio (d_d / t) and geometric diameter ratio (d_d / d_s) display considerable departure from spherical geometry. This causes a significant underestimate in the particle area and hence an overestimation of the SAD. This can be corrected by using Eq. 8 and the resulting SAD values ($(dP / dA)_{sample}$) are plotted as open circles in Fig. 3c. With the exception of the fraction containing particles of about 0.3 μm in diameter the particle shape is generally consistent across the size distribution. Thus for the Darling River sample changes in shape are not responsible for the trends in the SADD plot.

A limited number of fractions were examined by SEM for the Mt Bold A1 Soil sample. They indicate that the smallest particles (0.1 μm) have a high aspect ratio which could influence the SAD value considerably. Indeed this shape factor appears to reverse the trend that the smallest particles have the

Table 1
Mean particle dimensions measured using SdFFF and SEM on a number of particles from specified fractions collected across the SdFFF fractograms given in Fig. 3a, d. The numbers in brackets represent the standard deviations of the mean value (i.e. S.D. / $\sqrt{m}$) measured to two significant figures of the mean

(a) Darling River					
Elution time (min)	15–20	45–50	65–70	80–85	90–95
Diameter range (μm)	0.074–0.087	0.174–0.197	0.277–0.309	0.381–0.422	0.467–0.518
No. of particles m	6	7	18	10	14
d_s (μm)	0.08	0.19	0.29	0.40	0.49
A_{csa} (μm^2)	0.011 (1)	0.24 (3)	0.53 (6)	0.56 (8)	0.71 (7)
d_d (μm)	0.11 (1)	0.24 (3)	0.53 (6)	0.56 (8)	0.71 (7)
t (μm)	0.044 (5)	0.09 (2)	0.12 (2)	0.35 (9)	0.35 (5)
d_d / t	2.75	2.67	4.42	1.60	2.03
A_d / A_s	1.33 (7)	1.50 (17)	2.49 (21)	1.51 (18)	1.46 (13)
dP / dA_{sphere}	819	145	179	231	431
dP / dA_{sample}	630 (31)	96 (11)	74 (13)	154 (18)	308 (18)
(b) Mt Bold A1 Soil					
Elution time (min)	15–20	55–60	70–75		
Diameter range (μm)	0.087–0.102	0.258–0.289	0.359–0.399		
No. of particles m	8	4	38		
d_s (μm)	0.095	0.274	0.381		
A_{csa} (μm^2)	0.05 (1)	0.15 (5)	0.21 (3)		
d_d (μm)	0.25 (2)	0.41 (9)	0.48 (3)		
t (μm)	0.010 (1)	0.22 (16)	0.23 (3)		
d_d / t	25.00	1.86	2.08		
A_d / A_s	4.01 (26)	1.89 (34)	1.50 (8)		
dP / dA_{sphere}	125	97	80		
dP / dA_{sample}	31 (5)	51 (5)	53 (7)		

largest SAD. However, this calculation is based on the SEM sizing of only eight particles and the conclusions should be regarded with caution (Fig. 3f).

Significant numbers of particles larger than 1 μm in diameter were observed in this fraction. This indicates that the sample preparation method involving centrifugation did not remove all the larger particles. These would be eluted by the steric mechanism in the SdFFF separation thus resulting in a mixture of large and small particles in the early fractions. Since the SAD calculations are based on the normal mode separation equations appropriate for the smaller particles, this would further underestimate the area resulting in an even greater decrease in the corrected SAD compared to the apparent spherical based SAD. The fraction of larger particles present was not determined although they were not dominant.

The larger fraction examined (at about 0.38 μm) involved measuring 38 particles and the results should be more reliable. The shape indicators were all very similar to those of the Darling River sample. In addition there were no abnormally large particles present showing that steric problems were not present. It is possible that large shifts in the corrected SAD values would only be found in the smallest particle size fractions. This is supported by the few particles measured in a fraction at about 0.27 μm, but too few particles were measured for reliable comparisons between this and the 0.38-μm fraction to be made.

4.3. Analysis of elemental composition with SdFFF–ICP-MS

The hyphenated technique SdFFF–ICP-MS gives element composition based fractograms and size distributions [7]. This data which is displayed in Figs. 4 and 5 shows that there is a distinct change in the chemical composition across the size distribution for the Mt Bold A1 Soil but the variations in the Darling River sample are not so apparent. The most sensitive way of monitoring such changes are to plot certain element ratio distributions. In Fig. 6 the Fe/Al and Mg/Al molar ratios are plotted against particle diameter for the two samples. Since these samples are dominated by aluminosilicate minerals Al was chosen as the relatively constant major element to compare with the other more variable elements.

For the Mt Bold soil sample the Fe/Al ratio decreases rapidly from 0.08 to 0.2 μm then remains approximately constant from 0.2 to 0.5 μm (Fig. 6c). In contrast, the Mg/Al ratio is constant for the first section of the fractogram (<0.2 μm) before increasing significantly with size (Fig. 6d). A reasonable hypothesis to explain these trends would be to assign most of the Fe in the smaller particles to hydrous iron oxide coatings on the particles. Then the increase in Fe/Al ratio with decreasing particle size is due to an increase in the specific surface area as particle size decreases and possibly to a change in shape as noted in the section above. Since iron oxides strongly adsorb orthophosphate the initial decrease in SAD observed in the SADD plot could be explained by a corresponding decrease in the Fe coating density. If the trend in the SADD plot is indeed reversed, as suggested by the very limited shape information available, then the trends are due to the change in shape rather than a change in iron coating thickness. For a more definite resolution of this point more accurate shape data is required.

The increase in Mg/Al ratio above 0.2 μm indicates a change in mineralogy of the sample. For example, an increase in illite compared with kaolinite could produce such a trend (Fig. 6d). The EDX data collected from the individual particles across the size range for the Mt Bold soil also supports the ICP-MS results which is consistent with the hypothesis that kaolinite clay particles with iron oxide surface coatings dominate the smaller-size particles (see Fig. 7a) and the illites dominate the larger-size particles (see Fig. 7b). The largest clay particles contain aluminium, silicon, iron and potassium. These elements are consistent with the presence of illite particles which have a reasonably high ion-exchange capacity.

Since the SADD plot continues to decrease more gradually with size for the larger particles either this change in mineralogy has little effect on the orthophosphate adsorption characteristics or the shape factor negates any such effect (Fig. 3f). Again better geometric data is required to distinguish between these effects.

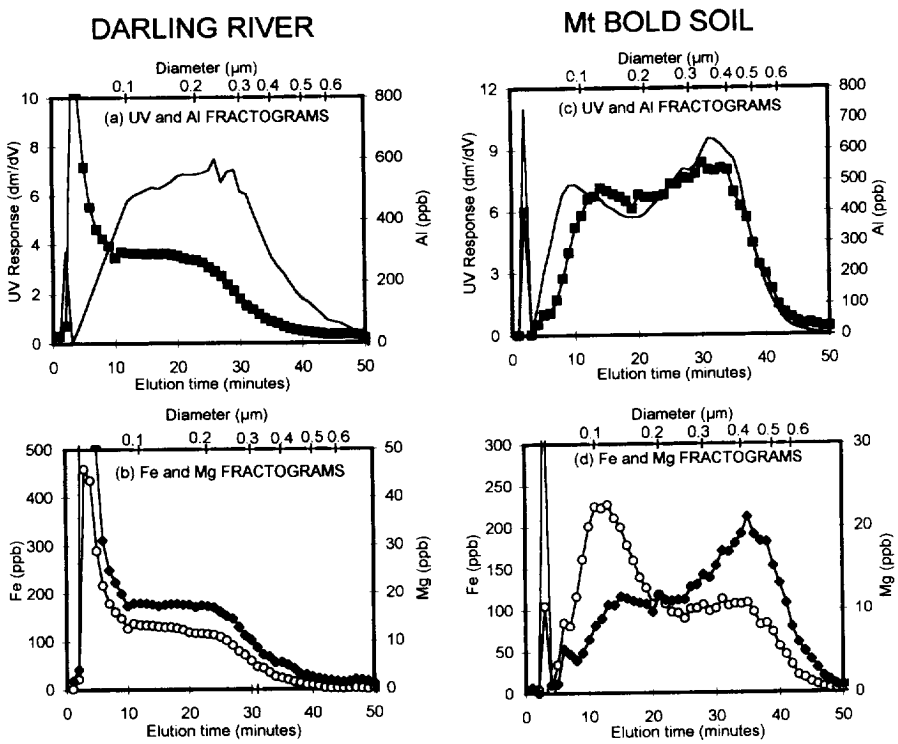

Fig. 4. Fractograms showing the SdFFF (system 2) separations. The solid lines give the UV detector response, the grey squares give the Al response (ppb), the black diamonds give the Mg response (ppb) and the open circles give the Fe response (ppb).

For the Darling River sample the trends in elemental ratio data are less distinct. The Fe/Al ratio decreases steadily and the Mg/Al ratio generally increases slightly across the entire diameter range (Fig. 6a, b). The individual trends do not appear to be enough to offer a clear explanation of the more pronounced shape of the SADD plot with its distinct minimum at about 0.2–0.3 μm. Perhaps a combination of factors or an as yet unknown effect is responsible for the SADD plot of the sample. This will be the subject of continuing research in our laboratory.

5. Conclusion

A SdFFF methodology is being developed that enables the surface adsorption density distribution of pollutants to be determined. The interpretation of the trends in these SADD plots requires information on changes in particle shape and chemical composition across the size distribution of the sample. The approach has been illustrated using the adsorption of ^{32}P-labelled orthophosphate onto samples of a river suspended colloid and a soil colloid. The shape was determined by SEM and the mineralogical trends using SdFFF–ICP-MS and EDX. A method has been derived to correct the apparent SAD values based on constant spherical geometry which accounts for the change in surface area for plate-like particles of measured dimensions. The major uncertainty is in the quality of the particle shape data which is determined by quite tedious SEM measurements. It is suggested that the changes in chemical composition observed across the size distribution could influence the trends in the SADD plots by two mechanisms. Firstly, a change in mineral type and, secondly, variations in the thickness of the highly adsorbing hydrous iron oxide surface coatings. The

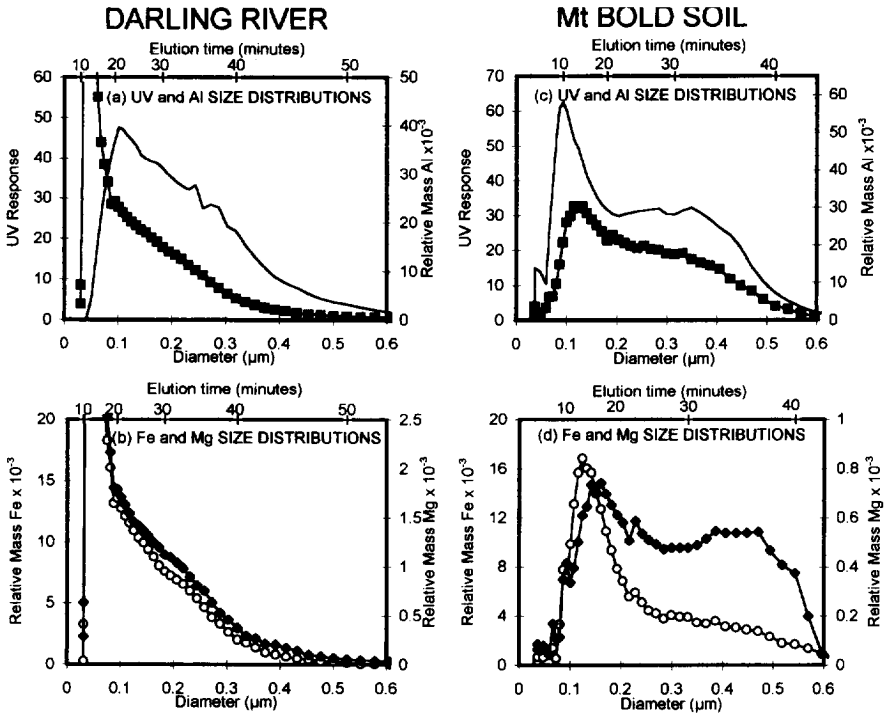

Fig. 5. The calculated mass and elemental based size distributions from the SdFFF (system 2) fractograms. The solid lines give the UV detector response, the grey squares give the Al response (ppb), the black diamonds give the Mg response (ppb) and the open circles give the Fe response (ppb).

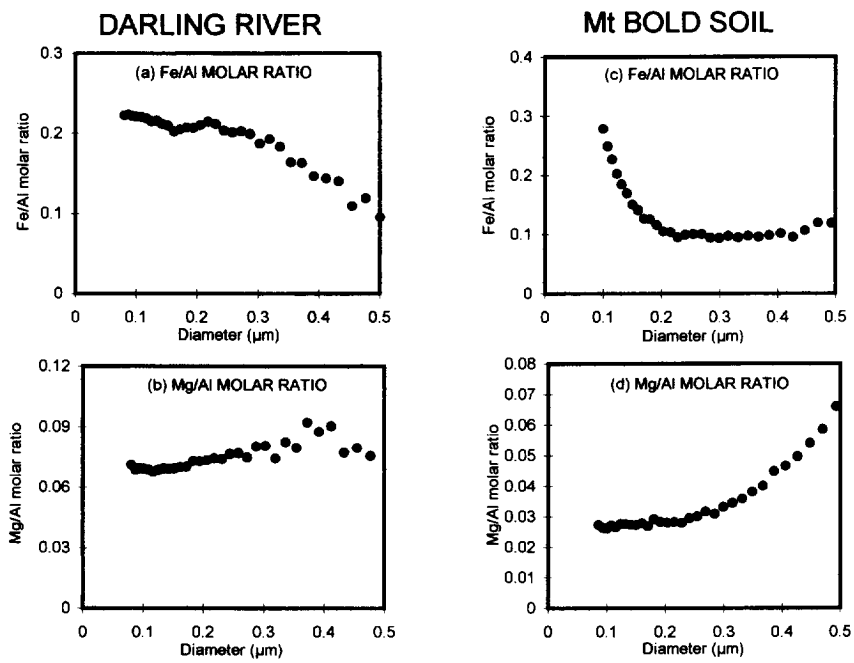

Fig. 6. Element Molar ratio versus particle diameter. (a) Fe/Al, (b) Mg/Al, (c) Fe/Al and (d) Mg/Al.

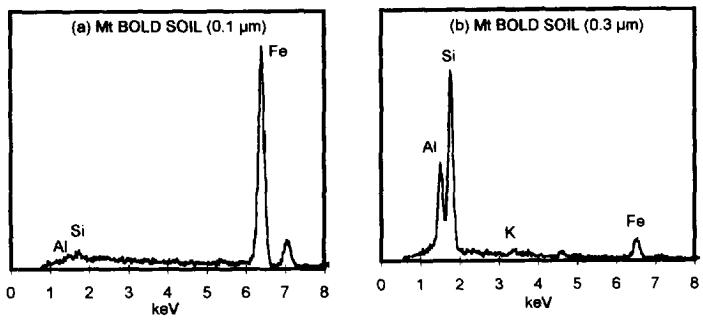

Fig. 7. Energy dispersive X-ray analysis (EDX) of individual particles from the SdFFF separation the Mt Bold soil sample. (a) 0.1 μm diameter particle and (b) 0.3 μm diameter particle.

method generates adsorption data of unprecedented detail which should be valuable in interpreting the phosphorus speciation and fate in natural waters and soils.

References

[1] R. Beckett, D.M. Hotchin and B.T. Hart, J. Chromatogr., 517 (1990) 435.
[2] R. Beckett, G. Nicholson, B.T. Hart, M. Hansen and J.C. Giddings, Water Res., 22 (1988) 1535.
[3] R. Beckett, G. Nicholson, D.M. Hotchin and B.T. Hart, Hydrobiologia, 235/236 (1992) 697.
[4] R. Beckett and B.T. Hart, in J. Buffle (Editor), Environmental Particles, Vol. 2, Lewis Publishers, Boca Raton, FL, 1993, pp. 165–205.
[5] J.C. Giddings, P.S. Williams and R. Beckett, Anal. Chem., 59 (1987) 28.
[6] P.S. Williams and J.C. Giddings, Anal. Chem., 59 (1987) 2038.
[7] D.M. Murphy, J.R. Garbarino, H.E. Taylor, B.T. Hart and R. Beckett, J. Chromatogr., 642 (1993) 459.
[8] D.T. Chittleborough, D.M. Hotchin and R. Beckett, Soil Sci., 153 (1992) 341.
[9] J.C. Giddings, Chem. Eng. News, 66 (1988) 34.
[10] K.R.J. Smettem, D.J. Chittleborough, B.G. Richards and F.W. Leaney, J. Hydrol., 122 (1991) 235–252.